

DAMPED Ly α ABSORBER AT HIGH REDSHIFT: LARGE DISKS OR GALACTIC BUILDING BLOCKS?

MARTIN G. HAEHNELT,¹ MATTHIAS STEINMETZ,² AND MICHAEL RAUCH^{3,4}

Received 1997 June 18; accepted 1997 October 20

ABSTRACT

We investigate the nature of the physical structures giving rise to damped Ly α absorption systems (DLAS) at high redshift. In particular, we examine the suggestion that rapidly rotating large disks are the only viable explanation for the characteristic observed asymmetric profiles of low-ionization absorption lines. Using hydrodynamic simulations of galaxy formation in a cosmological context, we demonstrate that irregular protogalactic clumps can reproduce the observed velocity width distribution and asymmetries of the absorption profiles equally well. The velocity broadening in the simulated clumps is the result of a mixture of rotation, random motions, infall, and merging. The observed velocity width correlates with the virial velocity of the dark matter halo of the forming protogalactic clump ($\Delta v \approx 0.6v_{\text{vir}}$ for the median values, with a large scatter, on the order of a factor of 2, between different lines of sight). The typical virial velocity of the halos required to give rise to the DLAS population is about 100 km s⁻¹, and most standard hierarchical structure formation scenarios can easily account for even the largest observed velocity widths. We conclude that the evidence that DLAS at high redshift are related to large, rapidly rotating disks with $v_{\text{circ}} \gtrsim 200$ km s⁻¹ is not compelling.

Subject headings: galaxies: kinematics and dynamics — galaxies: structure — intergalactic medium — quasars: absorption lines

1. INTRODUCTION

Damped Ly α absorption systems (DLAS) have often been interpreted as large high-redshift progenitors of present-day spirals that have evolved little apart from forming stars (Wolfe 1988; Lanzetta et al. 1991; Wolfe 1995; Wolfe et al. 1995; Lanzetta, Wolfe, & Turnshek 1995). A number of observational results have been cited in support of this hypothesis (see § 6 below). Most recently, Prochaska & Wolfe (1997) have investigated a variety of idealized models for the spatial distribution and kinematics of the absorbing gas to test whether they could reproduce the absorption line profiles of low-ionization ionic species (LIS) associated with DLAS. Of the models they investigated, only one in which the lines of sight (LOS) intersect rapidly rotating thick galactic disks can explain both the large velocity spreads (up to 200 km s⁻¹) and the characteristic asymmetries of the observed LIS absorption profiles. In particular, they find that if they embed their disk model within a cold dark matter (CDM) structure formation scenario, the result is inconsistent with the observed velocity widths. In this paper, we demonstrate that the inconsistency with galaxy formation models within hierarchical cosmologies (e.g., Kauffmann 1996) disappears if the gas is modeled with a more realistic spatial distribution and kinematic structure.

We use numerical simulations of galaxy formation in a CDM cosmology that includes gas dynamics and realistic initial conditions. These exhibit a complex relationship between high column density absorption features and the underlying dark matter distribution (Katz et al. 1996; Haehnelt, Steinmetz, & Rauch 1996, hereafter Paper I; Rauch, Haehnelt, & Steinmetz 1997, hereafter Paper II;

Gardner et al. 1997a, 1997b). Agglomerations of neutral hydrogen with central column densities larger than 10²⁰ cm⁻² and masses on the scale of dwarf galaxies do commonly occur in these simulations. These objects form by gravitational collapse in CDM potential wells. Subsequent cooling produces an optically thick, mostly neutral phase in the innermost 10 kpc. We have demonstrated earlier that the large number of these objects and their clustering and merging into larger units can explain many observed features of metal absorption systems—for example, the ionization and thermal state of the gas and the observed multicomponent structure of the absorption line profiles (Papers I and II). In these models, the high incidence rate of damped Ly α systems is a result of the high abundance of protogalactic clumps (PGC), which are the progenitors of large present-day galaxies. This must be contrasted with the popular picture of DLAS, in which a population of very large disks evolves without merging to form present-day spirals.

Prochaska & Wolfe (1997) have highlighted two crucial questions that a hierarchical structure formation model must be able to address satisfactorily:

1. How do the observed asymmetries of the absorption line complexes arise?
2. Can absorption by groups of PGCs in a hierarchical universe reproduce the observed velocity width distribution?

Below, we will investigate the velocity width and shape of LIS absorption profiles using artificial spectra for lines of sight through numerically simulated regions of ongoing galaxy formation. We then examine the underlying physical conditions responsible for the kinematic structure of these systems. We further investigate the connection between the velocity width of the absorption systems and the depth of the forming potential well and address the question of how to accommodate the observed velocity width within standard hierarchical cosmologies. Finally, we discuss our results and some other, observational clues to the nature of DLAS, and draw conclusions.

¹ Max-Planck-Institut für Astrophysik, Postfach 1523, 85740 Garching, Germany; mhaehnelt@mpa-garching.mpg.de.

² Steward Observatory, University of Arizona, Tucson, AZ 85721; steinmetz@as.arizona.edu.

³ Astronomy Department, California Institute of Technology, Pasadena, CA 91125; mr@astro.caltech.edu.

⁴ Hubble fellow.

2. NUMERICAL SIMULATIONS OF DAMPED Ly α SYSTEMS

2.1. The Hydrodynamical Simulations

Spatial regions of the universe selected to contain one or a few normal galaxies at redshift zero are simulated with the hydrodynamic GRAPESPH code (Steinmetz 1996) in the framework of a standard CDM cosmogony ($\sigma_8 = 0.67$, $H_0 = 50 \text{ km s}^{-1} \text{ Mpc}^{-1}$, $\Omega_b = 0.05$). Temperature, density, and peculiar velocity arrays along the LOS through the simulated boxes are used to produce artificial absorption spectra. For a detailed description of the properties of the simulations and the resulting absorption features, see Steinmetz (1996), Navarro & Steinmetz (1997), and Papers I and II. The strategy of simulating small regions of ongoing galaxy formation preselected from a large dark matter simulation allows us to achieve a spatial resolution of 1 kpc and a mass resolution of $5 \times 10^6 M_\odot$ (in gas). This high resolution—about a factor of 10 higher than in most other cosmological hydrosimulations—is crucial for resolving the rich substructure within the damped region induced by the frequent merging of protogalactic clumps in hierarchical structure formation scenarios. Despite this, the resolution is still not sufficient to account for a possible clumping on subkiloparsec scales due to thermal instabilities (Mo 1994; Mo & Miralda-Escudé 1996). Furthermore, energy and momentum feedback due to star formation are not included. Both effects should produce additional substructure in physical space. The effect of feedback from star formation on the amount of substructure in velocity space seems less obvious.

2.2. The Region of Neutral Hydrogen: Self-Shielding

To study the kinematic structure of damped systems, we extend our previous work to lines of sight passing through regions of collapsed dark matter halos with integrated H I column densities exceeding $2 \times 10^{20} \text{ cm}^{-2}$. The main problem then arising is the treatment of the self-shielding of the dense gas against radiation beyond the Lyman edge. With the current generation of computers, it is not yet possible to run cosmological hydrosimulations that solve the full radiative transfer equations. We have therefore adopted a simple scheme to mimic the effect of self-shielding, which is motivated by the tight correlation between column density and density predicted by the numerical simulations (Miralda-Escudé et al. 1996; Paper II). A H I column density of 10^{17} cm^{-2} , above which self-shielding becomes important, occurs for lines of sight with absorption-weighted densities of about 10^{-3} cm^{-3} to 10^{-2} cm^{-3} . This is easy to understand by looking at the photoionization equilibrium equation for a highly ionized, optically thin homogeneous slab of hydrogen. The column density of neutral hydrogen then scales as $N_{\text{HI}} \propto n_{\text{H}}^2 D J_{912}$, where D is the thickness of the slab and J_{912} is the flux of the UV background at the Lyman edge. The hydrogen density at the onset of self-shielding in the central plane can be written as

$$n_{\text{shield}} \sim 3 \times 10^{-3} \left(\frac{D}{10 \text{ kpc}} \right)^{-0.5} \times \left(\frac{J_{912}}{0.3 \times 10^{-21} \text{ ergs cm}^{-2} \text{ sec}^{-1} \text{ Hz}^{-1} \text{ sr}^{-1}} \right)^{0.5} \text{ cm}^{-3}, \quad (1)$$

where the spectral shape proposed by Haardt & Madau (1996) is used to transform the flux at the Lyman edge, J_{912} , into a photoionization rate. The geometry of collapsed regions in the numerical simulations is certainly more complicated than that of a slab, but $D = 10 \text{ kpc}$ is a typical scale. To be on the safe side, we assume that all the gas above a density threshold of 10^{-2} cm^{-2} is self-shielded. This probably underestimates the size of the self-shielding region.

2.3. Profiles of Low-Ionization Ionic Species

In observed DLAS, hydrogen is predominantly neutral, owing to the self-shielding of the gas, while the other atomic species attain low-ionization states (Viegas 1995). Optically thin transitions of LIS such as Si II, Al II, Fe II, and Ni II are therefore generally considered suitable tracers of the kinematic and density structure of the neutral gas (Wolfe 1995). We have chosen the Si II 1808 absorption feature for our investigation. Silicon was assumed to be predominantly in the first ionization state within the self-shielding region,

$$\frac{[\text{Si II}]}{[\text{Si}]} = 1 \quad n_{\text{H}} > 10^{-2} \text{ cm}^{-3},$$

$$\frac{[\text{Si II}]}{[\text{Si}]} = 0 \quad \text{otherwise}.$$

A homogeneous silicon abundance of $[\text{Si}/\text{H}] = -1$ was assumed for the self-shielding region. Artificial spectra were made to resemble typical Keck data obtainable within a few hours from a 16th–17th magnitude QSO (S/N = 50 per 0.043 \AA pixel, FWHM = 8 km s^{-1}). To connect this with our previous work, we will also show the corresponding C IV absorption line profiles. For these, a homogeneous carbon abundance of $[\text{C}/\text{H}] = -1.5$ was assumed. The C IV fraction was calculated using the photoionization code CLOUDY (Ferland 1993), as described in Papers I and II.

2.4. A Gallery of Simulated Damped Ly α Absorbers

Figures 1–5 present some typical examples of simulated damped Ly α absorption systems. The bottom left panel shows the absorption spectrum for the Si II 1808 and C IV 1548 transitions, the top left and bottom right panels show the total hydrogen density and peculiar velocity along the LOS, and the top right panel shows density and velocity fields in a thin slice containing the LOS. The coordinates are proper distance, and the projection is such that the LOS along which the absorption spectrum is determined lies along the z -axis. The wavelength axis of the spectra is in km s^{-1} . Velocities are relative to the center-of-mass velocity of a sphere with 30 kpc radius. The assumed density threshold for self-shielding is indicated by a dashed line in the density profile and by a thick contour in the slice of the density field.

Figure 1 shows a typical example of two merging PGCs. The density profile along the line of sight has two peaks within the self-shielding region. On larger scales, the gas is flowing in from the left and right, but in the self-shielded region, the flow is rather quiescent, with a velocity gradient of only about 30 km s^{-1} . This results in a double-peaked Si II 1808 absorption profile with about a 30 km s^{-1} velocity difference between the peaks.

Figure 2 shows another example of merging PGCs. This time, the density profile along the line of sight has three rather marginal peaks within the self-shielding region. The

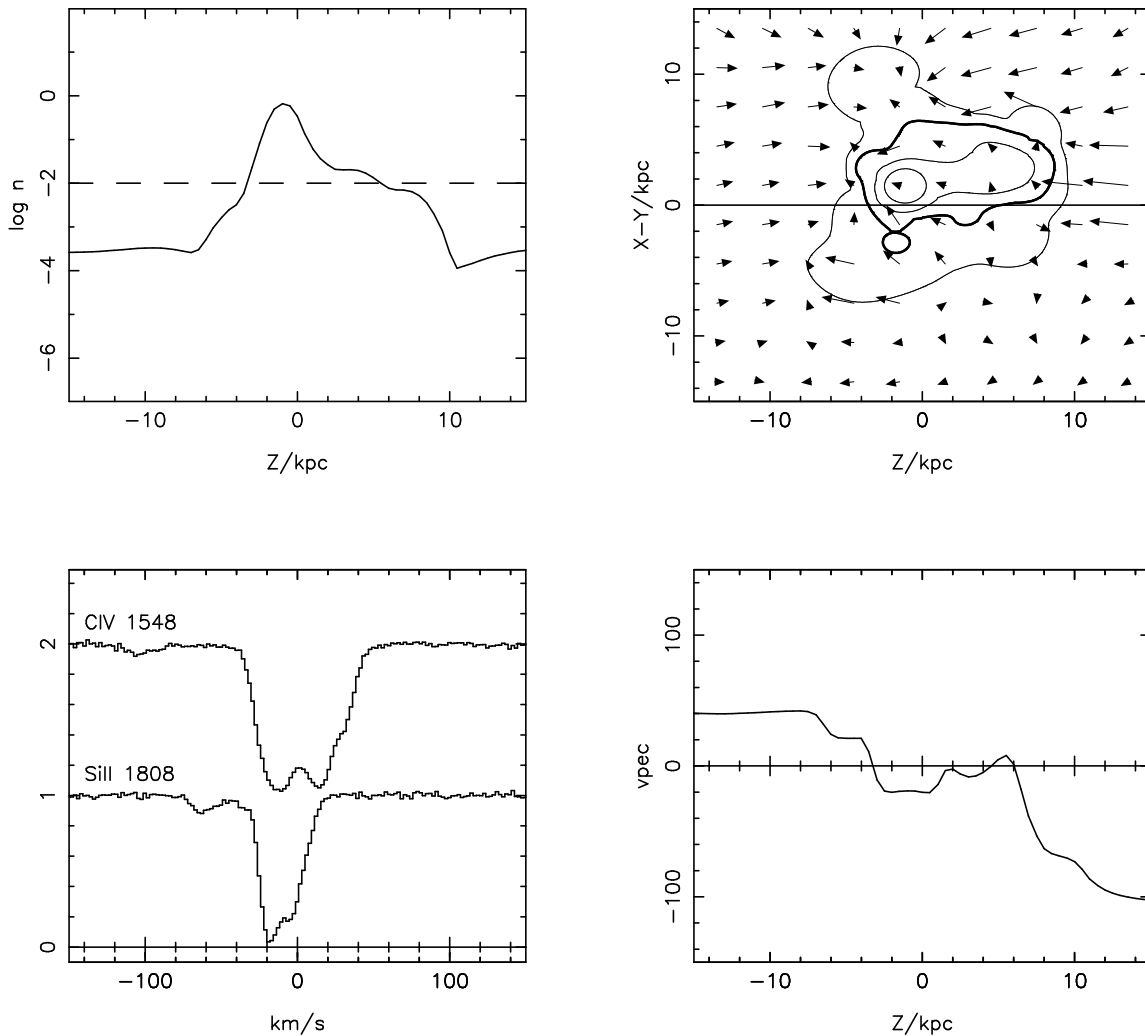


FIG. 1.—Simulated damped $\text{Ly}\alpha$ absorber at $z = 2.1$ with $\log N_{\text{H I}} = 21.2$, arising from gas in a merging protogalactic clump with $v_{\text{vir}} = 70 \text{ km s}^{-1}$. *Bottom left*: Absorption spectrum for the Si II 1808 and C IV 1548 transitions. *Top left*: Total hydrogen density along the LOS. *Bottom right*: Peculiar velocity along the LOS. *Top right*: Density and velocity field in a thin slice containing the LOS (straight solid line). The density contours have a spacing of 1 dex, and the thick contour marks $\log n = -2$. Velocities are relative to the center-of-mass velocity of a sphere with 30 kpc radius. The normalization of the velocity arrows is such that the length of the longest arrow equals the spacing between arrows. For absolute velocity values, see the bottom right panel.

velocity profile is smooth but shows large gradients due to an eddylike motion in the shock produced by the infalling clump. The corresponding Si II 1808 absorption profile is complex and extends over 200 km s^{-1} , showing a prominent leading edge. The hump in the velocity profile at 5 kpc and the three density peaks all show up as individual absorption features.

Figure 3 shows a third, similar example of merging PGCs. The peculiar velocity profile shows the same large gradients, but it is much more chaotic than that in Figure 2. The peaks of the density profiles and the features of the velocity profile in the self-shielding region can again be identified in the Si II 1808 absorption profile, which also shows a prominent leading edge. One should note here the strong difference between the Si II 1808 profile and the C IV 1548 profile. The latter arises from absorption by the spatially separated warm gas surrounding the self-shielding region.

Figures 4 and 5 show two of the rather rare cases in which there is a large rotational component in the motion of the gas. For these “rotating” PGCs, we generally find rather smooth density and velocity profiles in the self-

shielding region. In most cases, these result in single-peaked Si II 1808 absorption profiles with mild asymmetries or extended wings to one side, as shown in Figure 4. The latter are often difficult to detect unless the main peak is already saturated. The best example we could find of a leading-edge profile produced by rotation is shown in Figure 5.

2.5. Orientation Effects

As discussed above, the detailed structure of the absorption profile of the LIS regions depends strongly on the substructure in physical and velocity space. This makes the absorption profiles very sensitive to the orientation of the LOS. In order to demonstrate this, we plot in Figure 6 ten different randomly oriented lines of sight, each giving rise to damped $\text{Ly}\alpha$ absorption, in the vicinity of the PGC shown in Figure 1. The nature of the absorption profiles varies from a single symmetric peak to double and multiple peaks. The rapid changes in the details of the velocity profile along the LOS are due to the rather chaotic velocity field of the merging PGC, and are the main reason for the dramatic changes in the LIS absorption profile. It is also evident that the absorption profile of the higher ionization ion C IV

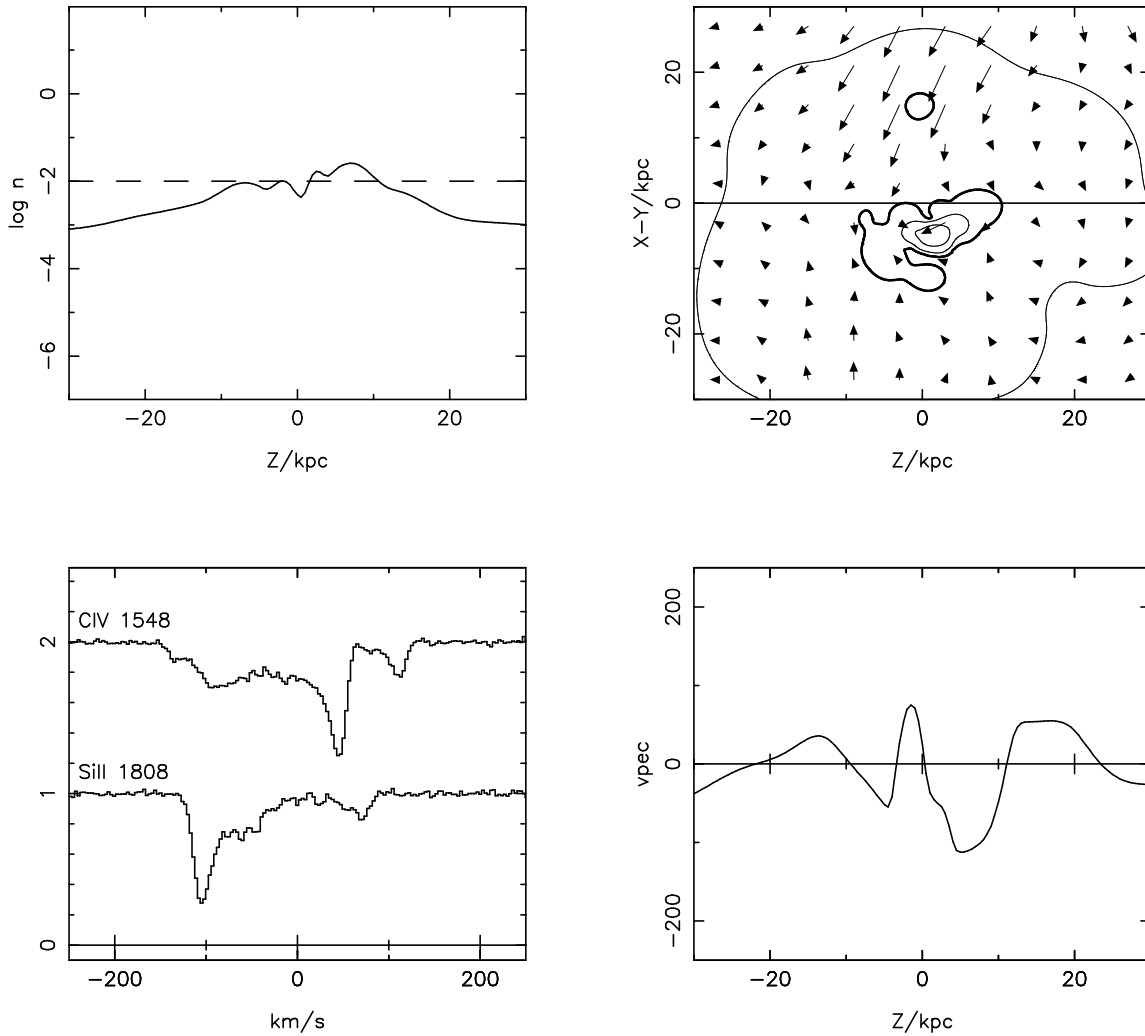


FIG. 2.—Same as Fig. 1, for simulated damped Ly α absorber at $z = 3.1$ with $\log N_{\text{H I}} = 20.6$, arising from gas in a merging protogalactic clump with $v_{\text{vir}} = 65 \text{ km s}^{-1}$.

varies independently of Si II. This is because C IV arises mainly from the warmer gas outside the self-shielding region.

3. DISTRIBUTION OF VELOCITY WIDTHS AND SHAPES: OBSERVED VS. SIMULATED

Prochaska & Wolfe (1997) have introduced four parameters to characterize LIS absorption profiles. In order to facilitate comparison with their observed sample of DLAS, we have applied their selection criteria and characterized the simulated LIS profiles in exactly the same manner. The Si II 1808 absorption profiles were transformed into an apparent optical depth profile, which was then smoothed over a range of nine pixels. The first parameter, the velocity width Δv of the LIS region, is defined as the velocity interval that contributes the central 90% to the optical depth-weighted velocity integral

$$\int \tau dv. \quad (2)$$

The mean velocity, v_{mean} , is defined as the midpoint of the velocity width interval (setting $v = 0$ at the left edge), while the median velocity, v_{med} , bisects the integral in equation (2)

performed over the velocity width interval. The three shape parameters, designed to detect asymmetries in the absorption complexes, are defined as

$$f_{\text{edg}} = \frac{|v_{\text{pk}} - v_{\text{mean}}|}{(\Delta v/2)} \quad (3)$$

$$f_{\text{mm}} = \frac{|v_{\text{median}} - v_{\text{mean}}|}{(\Delta v/2)} \quad (4)$$

$$f_{2\text{pk}} = \pm \frac{|v_{2\text{pk}} - v_{\text{mean}}|}{(\Delta v/2)}, \quad (5)$$

where v_{pk} and $v_{2\text{pk}}$ are the velocity of the highest and second-highest significant peak in the smoothed apparent optical depth profile. For the two-peak test, the plus (or minus) sign holds if the velocity of the second peak falls (does not fall) between the velocity of the first peak and the mean velocity. In the case of single peaks, $f_{2\text{pk}}$ is set equal to f_{edg} . To avoid saturation effects and to ensure a sufficient S/N ratio, only absorption profiles with

$$0.1 \leq \frac{I_{\text{pk}}}{I_0} \leq 0.6 \quad (6)$$

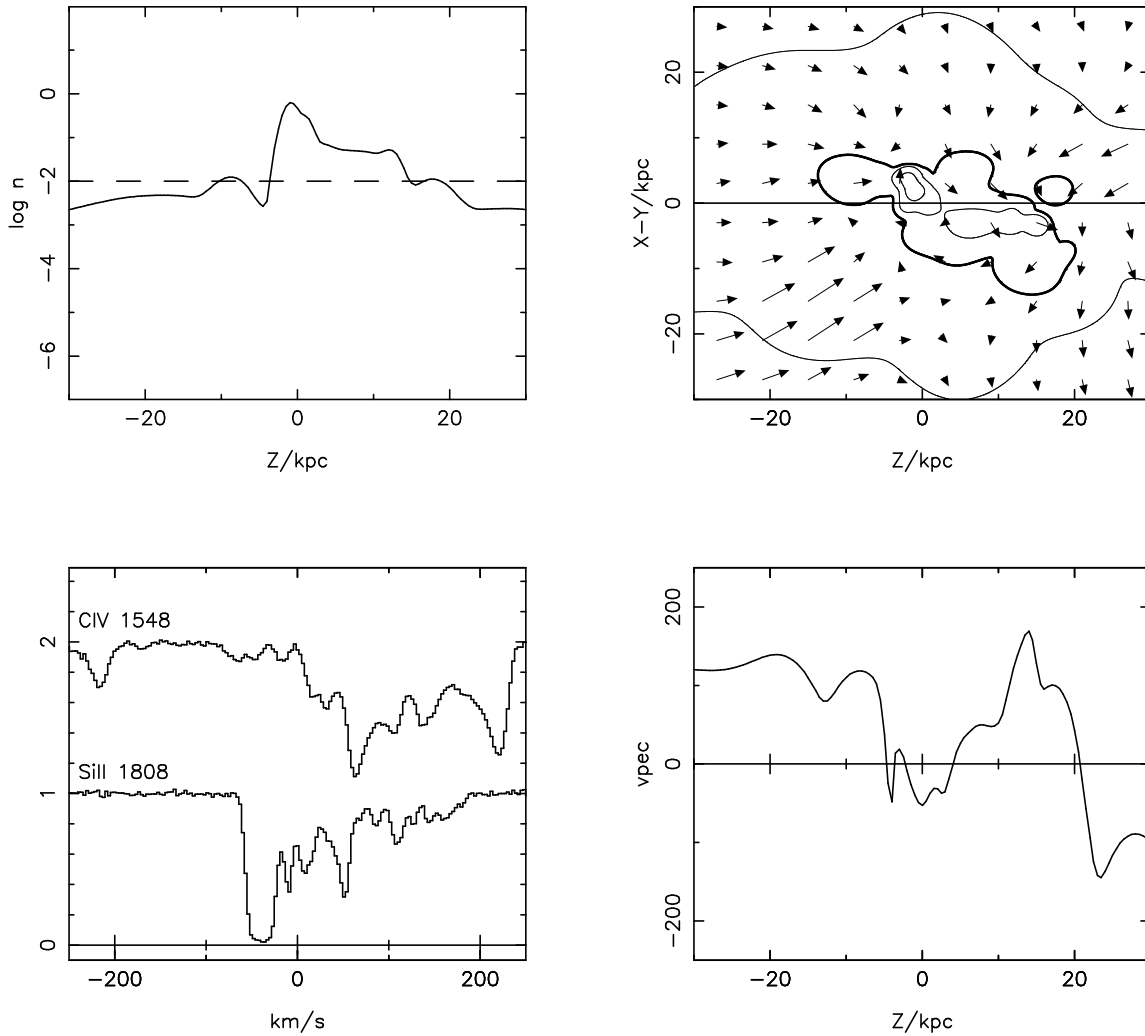


FIG. 3.—Same as Fig. 1, for simulated damped Ly α absorber at $z = 3.1$ with $\log N_{\text{H I}} = 21.7$, arising from gas in a merging protogalactic clump with $v_{\text{vir}} = 200 \text{ km s}^{-1}$.

were considered, where I_{pk} and I_0 are the intensity of the strongest peak and the continuum, respectively.

A sample of 640 simulated damped Ly α absorption systems with column densities above $2 \times 10^{20} \text{ cm}^{-2}$ and satisfying the criterion of equation (6) was assembled by choosing random lines of sight in the vicinity of 40 protogalactic clumps identified with a friends-of-friends group-finder. For the discussion of velocity widths, a minimum threshold of $\Delta v > 30 \text{ km s}^{-1}$ was imposed on both the observed and the simulated velocity widths, to avoid incompleteness effects. The redshift of the simulated DLAS is $z = 2.1$, the median redshift of the observed sample.

Figure 7 summarizes the comparison between the observed and simulated samples. The top panels show the differential distributions of the velocity width, the edge-leading, the mean-median, and the two-peak parameter. The observed sample is still small, and we therefore had to use rather large bins for the observed data. The absolute numbers of the observed sample are plotted, while the simulated sample is normalized accordingly. Error bars indicate the Poisson errors and the width of the bin, respectively. The velocity width is plotted relative to the median value of the observed sample and relative to the median value of subsamples of 16 lines of sight around each PGC in the

simulated sample. This allows us to test the relative velocity distribution independently of the cosmological model chosen. We return to the absolute velocity width of the LIS region in § 5. The bottom panels of Figure 7 show the corresponding cumulative distribution. The agreement between observed and simulated spectra is within the expected statistical errors. The Kolmogorov-Smirnov (K-S) test values for the cumulative distribution are given in Table 1. For none of the parameters is the K-S test probability smaller than 20%. We would, however, like to caution against using K-S tests to discriminate between different models. Small K-S probabilities can be very misleading if a

TABLE 1
K-S PROBABILITIES^a: OBSERVED
VS. SIMULATED

Test	Probability
$P_{\Delta v}$	0.69
P_{edg}	0.98
P_{mm}	0.23
$P_{2\text{pk}}$	0.28

^a K-S probabilities for Prochaska & Wolfe (1997) tests.

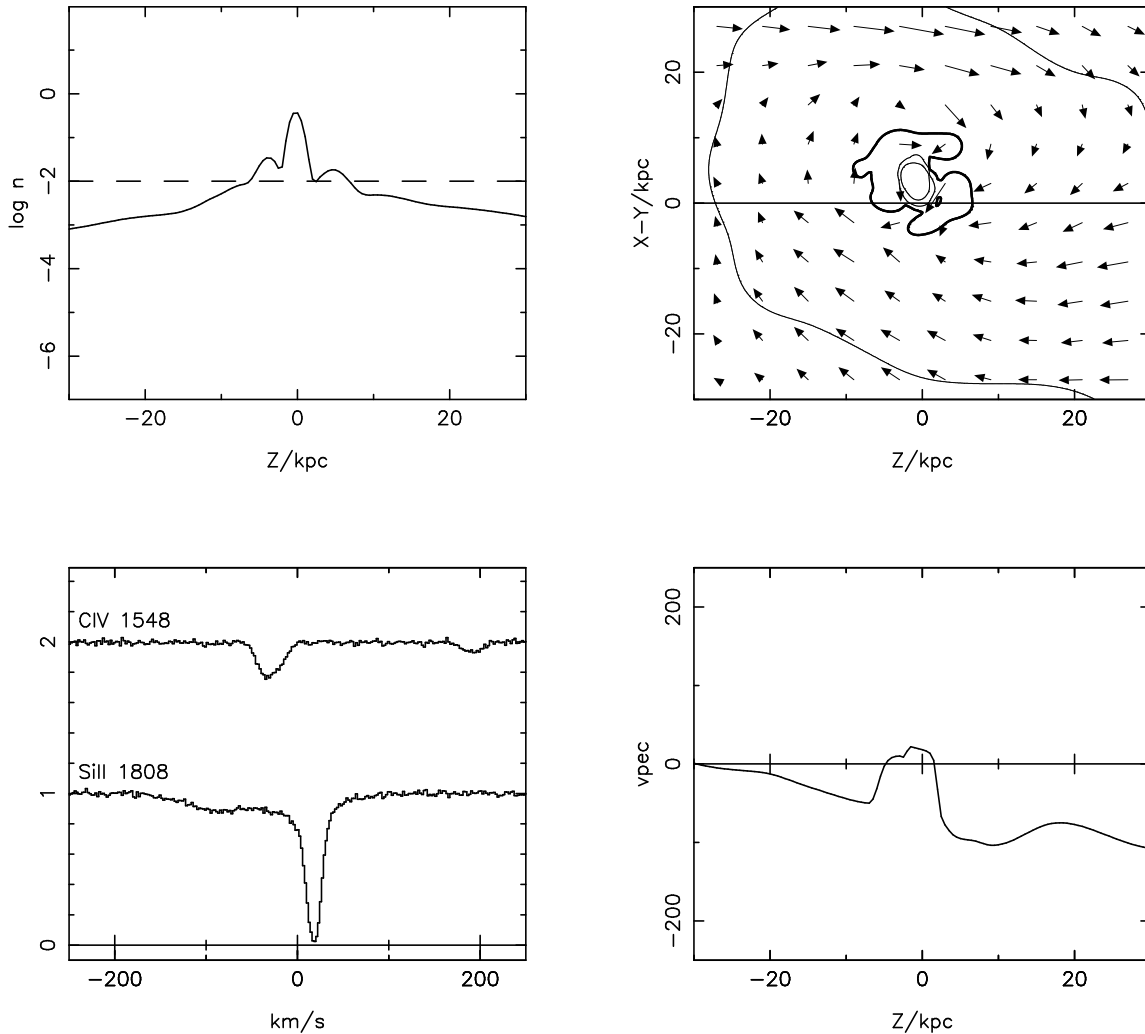


FIG. 4.—Same as Fig. 1, for simulated damped Ly α absorber at $z = 2.1$ with $\log N_{\text{H I}} = 21.3$, arising from gas in a “rotating” protogalactic clump with $v_{\text{vir}} = 180 \text{ km s}^{-1}$.

very special representation of a general class of models is chosen. We have, for example, varied our density threshold for the self-shielding region, the redshift of the sample, and the metallicity of the gas, and found significant changes in the distribution of the parameter. In some cases these changes further improved the agreement, and in some cases they led to K-S probabilities as small as 0.1% for one or two of the parameters. We believe that a significantly larger sample and a careful assessment of the selection effects are necessary in order to draw strong conclusions from the detailed distributions of the shape parameters introduced by Prochaska & Wolfe (1997).

4. PHYSICAL CONDITIONS GIVING RISE TO DAMPED Ly α SYSTEMS

In the previous section we have shown that lines of sight passing the vicinity of PGCs can give rise to DLAS with LIS absorption profiles that reproduce the characteristic velocity width distribution and asymmetries of observed DLAS. It remains to be seen which underlying physical conditions are giving rise to these features. In hierarchical structure formation scenarios, the “progenitor” of a present-day galaxy consists of several PGCs, often moving along filamentary structures to merge into larger objects.

We found the turbulent gas flows and inhomogeneous density structures related to the merging of two or more clumps to be the main reason for the occurrence of multiple LIS absorption systems with large velocity widths. Rotational motions of the gas play only a minor role for these absorption profiles, as does the velocity broadening due to the Hubble expansion between aligned clumps, which is important for higher ionization species like C IV (see Papers I and II). The latter is easily understandable given the small cross section of the LIS region.

4.1. Properties of the Absorbing Protogalactic Clumps

We have systematically investigated the physical properties of our sample of 40 PGCs in order to understand what kind of motions are reflected in the LIS line profiles and how their velocity width is related to the depth of the potential wells in which they are embedded. We have determined the following quantities for the absorbers: total velocity dispersion of the large-scale motions of the gas in the self-shielding region, velocity dispersion due to radial motions of the gas, overall rotational velocity of the gas, and virial velocity of the dark matter (DM) halo. The virial velocity is defined as $v_{\text{vir}} = (GM/r)^{1/2}$ in a sphere overdense by a factor of 200 compared to the mean cosmic density. One should

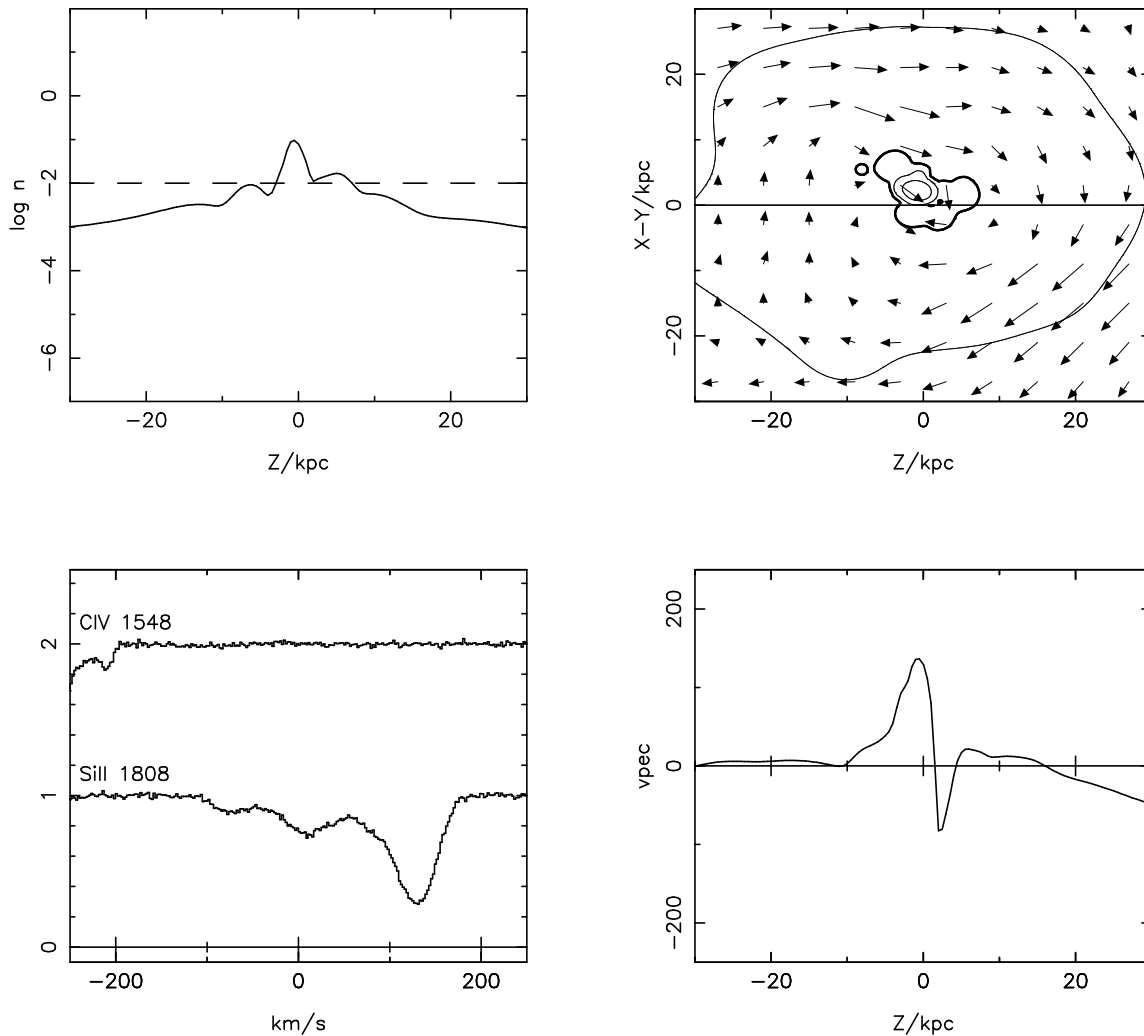


FIG. 5.—Same as Fig. 1, for simulated damped $\text{Ly}\alpha$ absorber at $z = 2.1$ with $\log N_{\text{H I}} = 20.8$, arising from gas in a “rotating” protogalactic clump with $v_{\text{vir}} = 180 \text{ km s}^{-1}$.

note here that the DM halo(s) are not necessarily virialized during the merger of two PGCs.

In Figure 8a, the median value of the velocity width for 16 randomly orientated lines of sight around each PGC is plotted against the virial velocity of the DM halo. There is a strong correlation, indicating that the velocity width reflects the depth of the potential reasonably well, even though there is considerable scatter. The velocity width of the LIS absorption region is typically 60% of the virial velocity of the DM halo. The solid line shows the least-squares fit.

Figure 8b shows the relation between rotational velocity and velocity width. There seems to be no correlation. The rotational velocity is generally too small to account for the observed LIS velocity width. In Figure 8c, the relative contribution of radial motions and rotation to the total velocity dispersion of the gas is shown. The contributions of rotation and radial motions (mainly infall and merging) range between 0% and 70%. As expected, these are anticorrelated. The contribution of additional random motions is generally between 30% and 70%.

4.2. How Do Asymmetric and Leading-Edge Profiles Arise?

The main motivation for interpreting observed absorption profiles as a signature of rotation are their leading

edges; i.e., the strongest absorption feature often occurs at one of the edges of the profile. As demonstrated by Prochaska & Wolfe (1997), such profiles occur naturally in a thick disk model with an exponential density and an isothermal velocity profile. Figure 5 shows one such example. There is, however, an equally simple and plausible explanation for these leading edges in a scenario of merging protogalactic clumps. In the case of two merging clumps, the strongest absorption feature will generally be caused by the high-density central region of the clump that is closest to the LOS. Smaller features are produced by density fluctuations in stripped material behind or shocked material in front of the dense region. This situation is illustrated schematically in Figure 9. Except in the rare case where the LOS passes both dense regions symmetrically, this is an intrinsically asymmetric configuration in velocity space, and the strongest absorption feature occurs naturally at the edge of the absorption profile. We find this configuration to be the principal reason for the occurrence of strongly asymmetric LIS absorption profiles in our models, but asymmetric infall and tidal tails do also contribute. We caution, however, against overinterpretation of leading-edge profiles. One should keep in mind that in the case of three randomly ordered components of varying strength, the probability

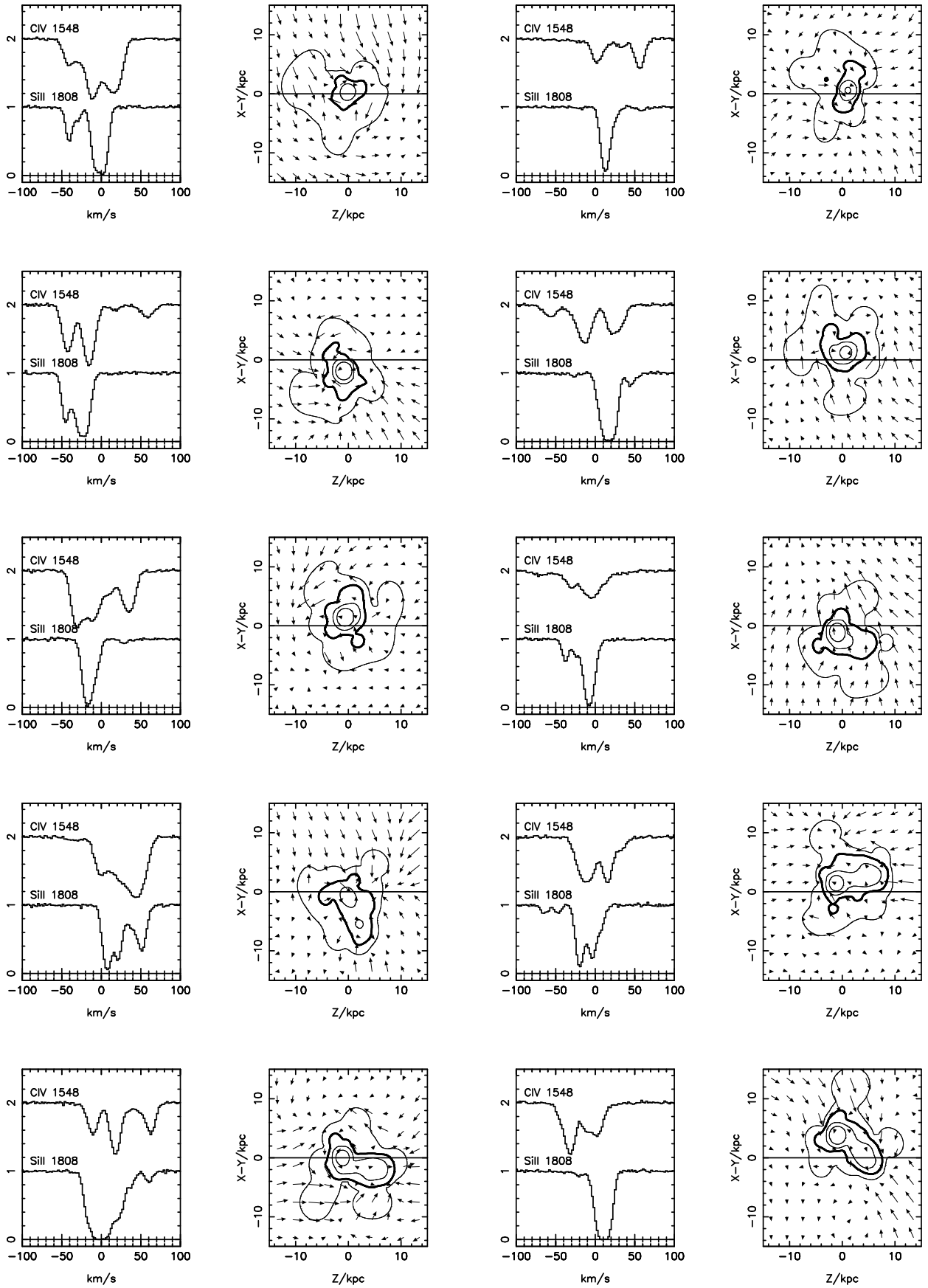


FIG. 6.—Ten random LOS producing damped Ly α absorption in the vicinity of the merging protogalactic clump shown in Fig. 1. Absorption spectra and corresponding density/velocity fields are plotted as in the top right and bottom left panels of Fig. 1.

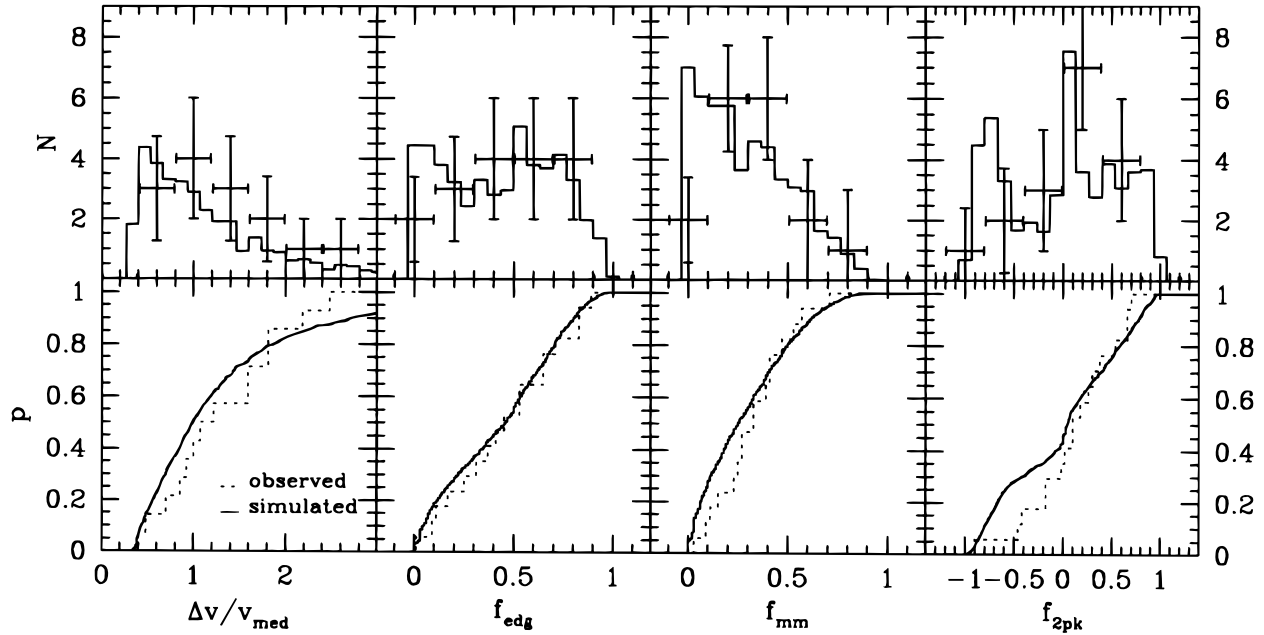


FIG. 7.—Velocity width distribution and shape parameters. *Left to right*: velocity width (relative to the median value), edge-leading index, mean-median index, and two-peak index. Top panels show the differential distribution in absolute numbers (model curves normalized to the observed number of systems); bottom panels show the cumulative probability distribution. Data are taken from Prochaska & Wolfe (1997).

that the strongest component is at one edge is $\frac{2}{3}$, and in the case of four components it is still $\frac{1}{2}$.

5. ABSOLUTE VELOCITY WIDTHS AND COSMOLOGICAL MODELS

In § 3 we have shown that the width distribution of the simulated LIS profiles relative to its median value is consistent with that observed, and in § 4.1 we demonstrated that the width of the profiles is correlated with the virial velocity of the associated DM halo. Figure 10a shows the complete velocity width distribution of the 640 DLAS in our sample. The median value is about 60% of the virial velocity of the associated DM halo,

$$\text{median}(\Delta v) \approx 0.6v_{\text{vir}}. \quad (7)$$

This value depends somewhat on the assumed density threshold for self-shielding, the assumed metallicity, the selection criterion of the PGC, and the redshift of the sample. Varying these parameters, we found the ratio of

velocity width to virial velocity to vary between 0.5 and 0.75. One should note here that the virial velocity that we infer from a given velocity width is a factor of 1.5 to 2.5 times smaller than in the rotating disk model.

It is difficult to be sure that the sample of PGCs picked from our numerical simulations is fully representative of the simulated cosmological model. Furthermore, to simulate a large number of different cosmogonies is very CPU time consuming. The exact velocity width distribution will depend on the distribution of virial velocities in a chosen cosmological model weighted by the cross section for damped absorption,

$$p(\Delta v, N_{\text{HI}} > N_{\text{damp}}, v_{\text{vir}}) = p(\Delta v | N_{\text{HI}} > N_{\text{damp}}, v_{\text{vir}}) \times p(N_{\text{HI}} > N_{\text{damp}} | v_{\text{vir}})p(v_{\text{vir}}). \quad (8)$$

We take the following approach to calculate the distribution of absolute velocity widths. The third factor in equation (8), the relative number of halos with different virial velocities, is calculated using the Press-Schechter for-

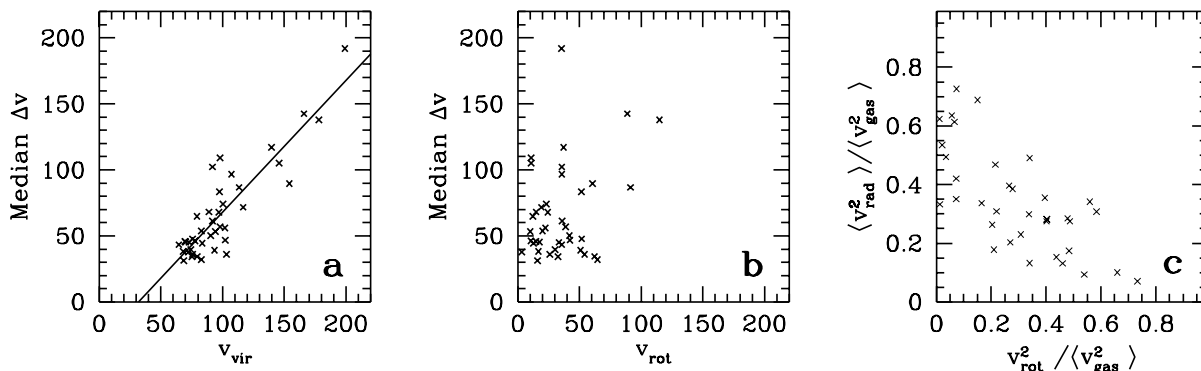


FIG. 8.—(a) Median velocity width of the LIS region for random lines of sight around 40 protogalactic clumps (median of 16 LOS per PGC) vs. virial velocity of the associated DM halo. (b) Median velocity width vs. mean rotational velocity of the gas. (c) Relative contributions of rotation and radial infall to the motion of the gas.

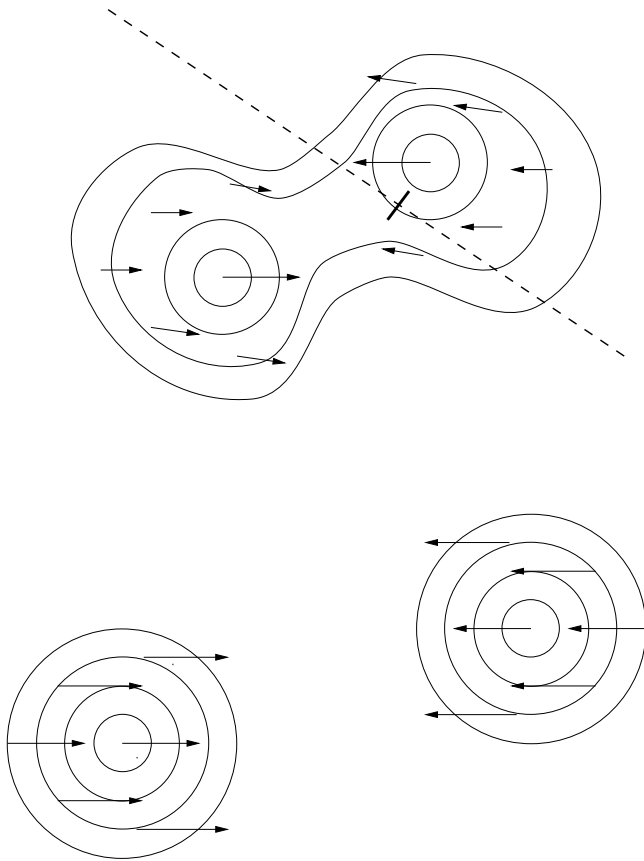
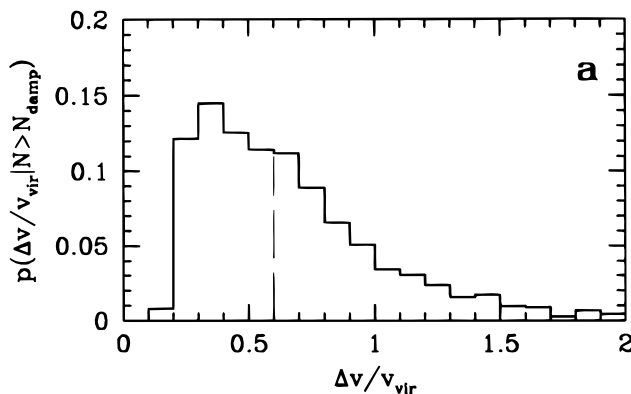


FIG. 9.—Schematic view of leading edges arising from merging protogalactic clumps. Dashed line represents a random line of sight, with the expected position of the strongest absorption feature marked.

malism (Press & Schechter 1974). The cross section for damped absorption is assumed to scale linearly with mass, $p(N_{\text{HI}} > N_{\text{damp}} | v_{\text{vir}}) \propto M \propto v_{\text{vir}}^3$. This is the simplest possible scaling suggested by the constant column density threshold defining a DLAS. A good estimate for the first factor can be obtained from our numerical simulations. We found that $p(\Delta v | N_{\text{HI}} > N_{\text{damp}}, v_{\text{vir}})$ depends mainly on the ratio of $\Delta v/v_{\text{vir}}$ and only weakly on the virial velocity of the dark matter halo itself. We therefore used the velocity width distribution of all 640 DLAS shown in Figure 10a. The distribution of absolute velocity widths is obtained by inte-



grating over virial velocity,

$$p(\Delta v, N_{\text{HI}} > N_{\text{damp}}) = \int_{v_{\text{min}}}^{\infty} p(\Delta v, N_{\text{HI}} > N_{\text{damp}}, v_{\text{vir}}) dv_{\text{vir}}. \quad (9)$$

The result is shown in Figure 10b for a standard CDM model at $z = 2.1$ with three different values of σ_8 and a minimum virial velocity of 30 km s^{-1} . Even the largest observed velocity width, $\sim 200 \text{ km s}^{-1}$, can be accommodated in a CDM model with σ_8 as low as 0.5 to 0.6. Most of the currently favored variants of hierarchical galaxy formation should therefore have no serious problems in accounting for the observed velocity width distribution. Constraints on different hierarchical scenarios by the overall incidence rate for damped absorption have been discussed extensively by other authors (see also § 6).

6. DAMPED $\text{Ly}\alpha$ ABSORBER: LARGE DISKS OR PROTOGALACTIC CLUMPS?

Current hydrodynamical simulations, including those presented here, are undoubtedly unable to model all the details of the spatial distribution and kinematics of the gas in the innermost regions of collapsed dark matter halos. We believe, however, that our simulations already catch many of the significant features and that, as discussed above, they underestimate rather than overestimate the amount of structure in the density and probably also in the velocity field. These simulations therefore cast serious doubt on the claim that only objects as massive as present-day spirals can produce the velocity widths of the observed LIS profiles, and that rotation is the only possible interpretation for the shape of the profiles. A number of other arguments have been put forward in favor of DLAS being large, protogalactic disks. We briefly comment on these here:

1. *High column densities:* Large H I column densities of DLAS are indeed reminiscent of present-day disks (e.g., Wolfe 1988). However, simple analytical estimates and the various simulations cited above show that these column densities can equally well be produced in gas-rich protogalactic clumps with masses as expected in typical hierarchical structure formation models.

2. *Large impact parameters:* Large separations between the absorber and detected emission attributed to associated starlight are taken to indicate extended, massive objects. However, very few absorbers at high redshift have been detected in emission (Møller & Warren 1995; Warren &

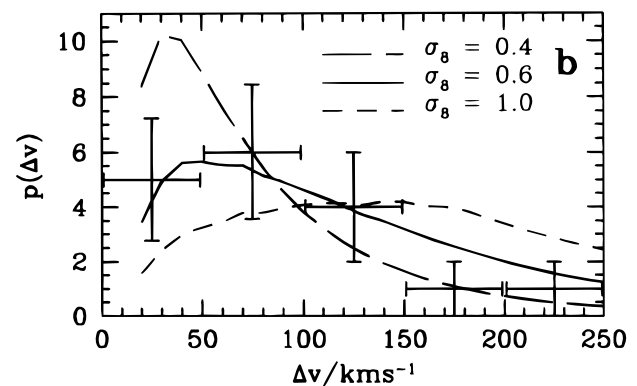


FIG. 10.—(a) Probability distribution of the velocity width scatter relative to the virial velocity of the associated DM halo of the PGC giving rise to the damped absorption system for 640 random lines of sight. Dashed line indicates the median value of 0.6. (b) Probability distribution of absolute velocity widths at $z = 2.1$ for CDM models with varying σ_8 , as indicated on the plot. Crosses show observed values from Prochaska & Wolfe (1997).

Møller 1995; Djorgovski et al. 1996; see also Le Brun, Bergeron, & Boissé [1996] and Le Brun et al. [1997] for observations of low- and intermediate-redshift DLAS in emission). It is not yet clear whether the inferred sizes actually contradict the predictions by hierarchical structure formation scenarios (Mo, Mao, & White 1997). This will depend crucially on the detailed gas distribution in the outskirts of protogalactic clumps. Moreover, we do not yet know how emission and absorption properties are related. As demonstrated in Papers I and II, regions of ongoing galaxy formation often contain several protogalactic clumps within a few tens of kpc.

3. *Continuity of Ω_b* : The integrated Ω_b in the H I phase of high-redshift DLAS is roughly similar to that in the stellar component of present-day spirals (Wolfe et al. 1986; Lanzetta et al. 1995; Storrie-Lombardi, McMahon, & Irwin 1996). However, this continuity may just mean that the gas constituting the stars observed today has already cooled and settled into collapsed objects at these redshifts. The integrated Ω_b contains no information about the size distribution of the collapsed objects. Hierarchical models have been shown to reproduce the observed Ω_b in DLAS and its evolution with redshift (Kauffmann & Charlot 1994; Ma & Bertschinger 1994; Mo & Miralda-Escudé 1994; Klypin et al. 1995; Gardner et al. 1997a, 1997b; Ma et al. 1997).

4. *Alignment of the edge of the absorption profile with the redshift of observed emission*: For two of the DLAS where emission has been observed, it is possible to determine the relative position of emission and absorption in redshift space (Lu, Sargent, & Barlow 1997). In the first case, the emission redshift coincides with one edge of the LIS absorption profile, while in the second case it lies roughly at the center of the absorption profile. For a rotating disc, the emission redshift should indeed occur preferentially at one of the edges of the LIS absorption profile if the center of emission coincides with the center of the disk and if there are no optical depth effects. The situation is, however, similar for the merging or collision of PGCs. The emission of a stellar continuum would most likely originate in one of the central regions of the merging clumps and should therefore also coincide with one of the two edges of the absorption profile.

For completeness, we mention a counterargument against massive disks that has received some attention in the past, the issue of the metallicities in DLAS. The metal abundances ($[Fe/H]$) in DLAS at high redshift are much lower than expected for local spiral disks (Pettini et al. 1994; Lanzetta, Wolfe, & Turnshek 1995; Lu et al. 1996;

Prochaska & Wolfe 1996; Pettini et al. 1997), which has led to suggestions that DLAS show abundance patterns of dwarf galaxies or galactic halos.

7. CONCLUSIONS

We have used hydrodynamical simulations of galaxy formation in a cosmological context to study the line profiles of low-ionization species associated with damped Ly α absorption systems. Observed velocity widths and asymmetries of the line profiles of the low-ionization species are well reproduced by a mixture of rotation, random motions, infall, and merging of protogalactic clumps. The asymmetries are mainly caused by random sampling of irregular density and velocity fields of individual halos and by intrinsically asymmetric configurations arising when two or more clumps collide. We show why leading-edge asymmetries occur naturally in the latter case; the dense central regions of the clumps move faster than surrounding less dense material.

We have further shown that the presence of noncircular motions reduces the depth of the potential well necessary to produce a given velocity width as compared to a model in which the absorption is solely due to rotation. The reduction is typically a factor of about 2. The observed velocity width can therefore be explained by gas moving into and within (forming) dark matter halos with typical virial velocities of about 100 km s $^{-1}$. Velocity width and virial velocity are linearly correlated, but the scatter is large; there are outliers with large velocity widths arising from an occasional alignment of clumps with well-separated dark matter halos.

Our final conclusion is that asymmetric profiles of the kind observed are not necessarily the signature of rotation, and that there is no problem in accommodating the observed velocity widths within standard hierarchical cosmologies.

We thank Simon White for a careful reading of the manuscript, Limin Lu, Hojun Mo, Jason Prochaska, and Art Wolfe for useful discussions, and the referee for a helpful report. M. R. is grateful to NASA for support through grant HF-01075.01-94A from the Space Telescope Science Institute, operated by the Association of Universities for Research in Astronomy, Inc., under NASA contract NAS 5-26555. Support by NATO grant CRG 950752 and the Sonderforschungsbereich 375-95 für Astro-Teilchenphysik der Deutschen Forschungsgemeinschaft is also gratefully acknowledged.

REFERENCES

- Djorgovski, S. G., Pahre, M. A., Bechtold, J., & Elston, R. 1996, *Nature*, 382, 234
 Ferland, G. J. 1993, University of Kentucky Dept. of Physics and Astronomy, Internal Report (Lexington: Univ. Kentucky)
 Gardner, J. P., Katz, N., Hernquist, L., & Weinberg, D. H. 1997a, *ApJ*, 484, 31
 Gardner, J. P., Katz, N., Weinberg, D. H., & Hernquist, L. 1997b, *ApJ*, 486, 42
 Haardt, F., & Madau, P. 1996, *ApJ*, 461, 20
 Haehnelt, M. G., Steinmetz, M., & Rauch, M. 1996, *ApJ*, 465, L95 (Paper I)
 Katz, N., Weinberg, D. H., Hernquist, L., & Miralda-Escudé, J. 1996, *ApJ*, 457, L57
 Kauffmann, G. A. M. 1996, *MNRAS*, 281, 475
 Kauffmann, G. A. M., & Charlot, S. 1994, *ApJ*, 430, L97
 Klypin, A., Borgani, S., Holtzman, J., & Primack, J. 1995, *ApJ*, 444, 1
 Lanzetta, K. M., Wolfe, A. M., & Turnshek, D. A. 1995, *ApJ*, 440, 435
 Lanzetta, K. M., Wolfe, A. M., Turnshek, D. A., Lu, L., McMahon, R. G., & Hazard, C. 1991, *ApJS*, 77, 1
 Le Brun, V., Bergeron, J., & Boissé, P. 1996, *A&A*, 306, 691
 Le Brun, V., Bergeron, J., Boissé, P., & Deharveng, J. M. 1997, *A&A*, 321, 733
 Lu, L., Sargent, W. L. W., & Barlow, T. A. 1997, *ApJ*, 484, 131
 Lu, L., Sargent, W. L. W., Barlow, T. A., Churchill, C. W., & Vogt, S. 1996, *ApJS*, 107, 475
 Ma, C.-P., & Bertschinger, E. 1994, *ApJ*, 434, L5
 Ma, C.-P., Bertschinger, E., Hernquist, L., Weinberg, D. H., & Katz, N. 1997, *ApJ*, 484, L1
 Miralda-Escudé, J., Cen, R., Ostriker, J. P., & Rauch, M. 1996, *ApJ*, 471, 582
 Mo, H. J. 1994, *MNRAS*, 269, 49
 Mo, H. J., & Miralda-Escudé, J. 1994, *ApJ*, 430, L25
 ———. 1996, *ApJ*, 469, 589
 Mo, H. J., Mao, S., & White, S. D. M. 1997, in preparation
 Møller, P., & Warren, S. J. 1995, in *Galaxies in the Young Universe*, ed. H. Hippelein, K. Meisenheimer, & H.-J. Röser (New York: Springer), 88
 Navarro, J. F., & Steinmetz, M. 1997, *ApJ*, 478, 13

- Pettini, M., Smith, L. J., Hunstead, R. W., & King, D. L. 1994, *ApJ*, 426, 79
- Pettini, M., Smith, L. J., King, D. L., & Hunstead, R. W. 1997, *ApJ*, 486, 665
- Press, W. H., & Schechter, P. L. 1974, *ApJ*, 187, 425
- Prochaska, J. X., & Wolfe, A. M. 1996, *ApJ*, 470, 403
- . 1997, *ApJ*, 487, 73
- Rauch, M., Haehnelt, M. G., & Steinmetz, M. 1997, *ApJ*, 481, 601 (Paper II)
- Steinmetz, M. 1996, *MNRAS*, 278, 1005
- Storrie-Lombardi, L. J., McMahon, R. G., & Irwin, M. J. 1996, *MNRAS*, 283, L79
- Viegas, S. M. 1995, *MNRAS*, 276, 268
- Warren, S. J., & Møller, P. 1995, in *IAU Symp. 171, New Light on Galaxy Evolution* (Dordrecht: Kluwer), in press
- Wolfe, A. M. 1988, in *QSO Absorption Lines: Probing the Universe*, ed. J. C. Blades, D. A. Turnshek, & C. A. Norman (Cambridge: Cambridge Univ. Press)
- . 1995, in *QSO Absorption Lines, Proc. ESO Workshop*, ed. G. Meylan (Berlin: Springer), 13
- Wolfe, A. M., Lanzetta, K. M., Foltz, C. B., & Chaffee, F. H. 1995, *ApJ*, 454, 698
- Wolfe, A. M., Turnshek, D. A., Smith, H. E., & Cohen, R. D. 1986, *ApJS*, 61, 249